

Photoluminescence probing of interface evolution with annealing in InGa(N)As/GaAs single quantum wells

Jun Shao,^{1,a)} Zhen Qi,¹ H. Zhao,² Liang Zhu,¹ Yuxin Song,³ Xiren Chen,¹ F.-X. Zha,⁴ Shaoling Guo,¹ and S. M. Wang^{2,3,b)}

¹National Laboratory for Infrared Physics, Shanghai Institute of Technical Physics, Chinese Academy of Sciences, 200083 Shanghai, China

²Department of Microtechnology and Nanoscience, Chalmers University of Technology, S-41296 Göteborg, Sweden

³State Key Laboratory of Functional Materials for Informatics, Shanghai Institute of Microsystem and Information Technology, Chinese Academy of Sciences, 200050 Shanghai, China

⁴Physics Department, Shanghai University, 200444 Shanghai, China

(Received 28 July 2015; accepted 10 October 2015; published online 23 October 2015)

The effects of thermal annealing on the interfaces of InGa(N)As/GaAs single quantum wells (SQWs) are investigated by excitation-, temperature-, and magnetic field-dependent photoluminescence (PL). The annealing at 750 °C results in more significant blueshift and narrowing to the PL peak than that at 600 °C. Each of the PL spectra can be reproduced with two PL components: (i) the low-energy component (LE) keeps energetically unchanged, while the high-energy component (HE) moves up with excitation and shows at higher energy for the In_{0.375}Ga_{0.625}As/GaAs but crosses over with the LE at a medium excitation power for the In_{0.375}Ga_{0.625}N_{0.012}As_{0.988}/GaAs SQWs. The HE is broader than the corresponding LE, the annealing at 750 °C narrows the LE and HE and shrinks their energetic separation; (ii) the PL components are excitonic, and the InGaNAs shows slightly enhanced excitonic effects relative to the InGaAs SQW; (iii) no typical *S-shape* evolution of PL energy with temperature is detectable, and similar blueshift and narrowing are identified for the same annealing. The phenomena are mainly from the interfacial processes. Annealing improves the intralayer quality, enhances the interfacial In-Ga interdiffusion, and reduces the interfacial fluctuation. The interfacial interdiffusion does not change obviously by the small N content and hence similar PL-component narrowing and blueshift are observed for the SQWs after a nominally identical annealing. Comparison with previous studies is made and the PL measurements under different conditions are shown to be effective for probing the interfacial evolution in QWs.

© 2015 AIP Publishing LLC. [<http://dx.doi.org/10.1063/1.4934523>]

I. INTRODUCTION

Photoluminescence (PL) as a powerful optical spectroscopy has been widely applied in characterizing semiconductors and quantum well (QW) structures,^{1,2} of which the transition energy, intensity, and linewidth have been frequently employed for extracting physical properties.^{3–6} With improved spectral resolution and signal-to-noise ratio (SNR), curve fitting analysis of PL spectrum can be performed, which provides more details about the PL processes involved and the competition in between,^{7,8} using different experimental conditions of excitation-power, temperature and magnetic field, bandedge electronic structure, shallow impurity levels, and/or interfacial process can be identified.^{9,10}

Dilute nitride In_xGa_{1-x}N_yAs_{1-y} has been extensively studied because of the large bandgap bowing and applications for GaAs-based telecom lasers.^{11–14} The optical quality deteriorates significantly with increasing N content due to the formation of deep levels with an associated *S-shape* evolution of transition energy in temperature-dependent PL measurements, and the *S-shape* diminishes with In content *x* and vanishes when *x* ≥ 0.3.^{15,16} To improve the optical quality, either *in*

situ annealing or post-growth rapid thermal annealing (RTA) is necessary, at the expense of a wavelength blueshift.¹⁷ As PL is more sensitive to the change in composition profile than other methods, such as X-ray diffraction,^{18,19} it was frequently used for clarifying the blueshift.^{20,21} The evolution of PL peak energy manifested pronounced *S-shape* for the dilute-N InGaNAs/GaAs single quantum wells (SQWs) at low temperatures, and followed the empirical Varshni model in the high-temperature region with significant reduction in the temperature dependence as compared to the N-free sample.^{22–25} However, (i) controversies remained that while the drastic blueshift after annealing was considered as a result of the N content and/or the N-related localized level in the QW layer but not the In-Ga interdiffusion,^{20,23,24} it was indicated that the annealing alone may induce interdiffusion in a length of ≤ 2 nm;²⁵ and (ii) while an exciton binding energy was derived to be about 6.5 meV for In_{0.05}Ga_{0.95}As/GaAs QW with a 8-nm-thick well layer,²⁶ a very small N content of about 0.5% in a 6-nm In_{0.4}Ga_{0.6}N_{0.005}As_{0.995}/GaAs SQW was shown to increase surprisingly the exciton binding energy by nearly 80% relative to the referential InGaAs/GaAs SQW to a value of about 17.5 meV.²⁷

In this work, the RTA effects on InGa(N)As/GaAs SQWs are characterized by PL measurements at different

^{a)}Electronic mail: jshao@mail.sitp.ac.cn

^{b)}Electronic mail: shum@mail.sim.ac.cn

excitations, temperatures, and magnetic fields, with the assistance of PL component analysis and bandedge electronic structure calculation. While no typical *S-shape* evolution of PL-peak energy with temperature is detectable, the PL peak blueshifts at similar levels for both the InGa(N)As SQWs after the same annealing. The PL spectra are well reproduced by a two-PL-component assumption, and the PL components are excitonic and of interband ground-state transition. Incorporation of dilute nitrogen into the QW layer moderately increases the exciton binding energy and reduced effective mass. Annealing improves interlayer crystal quality, enhances interfacial interdiffusion, and reduces the QW thickness and the interface fluctuation. Comparison suggests that PL measurements under different conditions with aid of curve fitting analysis may serve as an efficient vehicle for probing the interfacial evolution in QWs. The paper is organized as follows: In Sec. II, brief introduction is made to the PL experiments as well as the sample structures and RTA conditions. In Sec. III, excitation-power dependent PL analysis is first conducted, followed by magneto-PL analysis in Sec. III B, temperature-dependent investigation in Sec. III C, and mechanism discussion in Sec. III D. A conclusion is given in Sec. IV.

II. EXPERIMENT

Two $\text{In}_x\text{Ga}_{1-x}\text{As}/\text{GaAs}$ (denoted by A hereafter) and $\text{In}_x\text{Ga}_{1-x}\text{N}_y\text{As}_{1-y}/\text{GaAs}$ (denoted by B) SQW structures were grown on (100) GaAs substrate by an EPI930 molecular beam epitaxial system. The structure starts with a 200-nm GaAs buffer layer followed by a 100-nm $\text{Al}_{0.2}\text{Ga}_{0.8}\text{As}$ layer, the active region consists of a 24 monolayer (ML) thick InGa(N)As QW sandwiched between two 100-nm GaAs barrier layers. Another 100-nm $\text{Al}_{0.2}\text{Ga}_{0.8}\text{As}$ layer and a 10-nm GaAs cap layer were grown above. The growth temperature was 580 °C for the GaAs buffer and AlGaAs cladding layer, and 450 °C for the QW layer. The growth rates of InAs and GaAs were 0.5 and 1.0 ML/s, respectively. The In content x was characterized by rocking curve analysis as 0.375, and the thickness of the QW layer was about 7 nm. The structure B was grown with nitrogen (N) source open during the growth of QW layer, and the N content y was derived as 1.2%.¹⁷ Each of the structures was cut into three samples, of which one was taken as a reference (labeled by A/B-ag), and the other two were treated by post-growth rapid thermal annealing under 600 and 750 °C for 30 s (by A/B-600 and A/B-750). More details can be found elsewhere.¹⁷

PL measurements were performed with a Fourier transform infrared spectrometer-based PL system.² The spectrometer was equipped with an InGaAs photodiode detector and worked in the continuous-scan rather than step-scan mode.^{8,28} An Ar^+ -ion laser configured at 514.5 nm line was used for pumping, and the laser beam was focused on the sample with a diameter of about 0.5 mm, the power was exactly adjusted with a laser power controller in a range of 2–128 mW (equivalently, a power density range of 1–64 W/cm^2) for the excitation power-dependent PL measurements. A spectral resolution of 0.5 or 1.0 meV was set for the temperature/excitation-power or magnetic-field dependent measurements. A

close-cycle cryostat was used for the samples' temperatures of 11–300 K, its position was controlled to warrant the PL intensity a comparable quantity. A magneto-optical superconducting magnet in Faraday configuration^{10,29} was employed for the magneto-PL measurements at 4.5 K.

III. RESULTS AND DISCUSSION

Figure 1 illustrates the representative PL spectra of the InGaAs (A-ag, A-600 and A-750) and InGaNAs (B-ag, B-600 and B-750) SQWs at 11 K. Also plotted are the curve fittings of the spectra in dots, dashed-dots, and dashes.

The PL spectra show asymmetric lineshapes, and each can be reproduced by two PL components with Gaussian profile. Incorporation of nitrogen leads to an obvious redshift of the PL peak. The 600 °C annealing reduces the peak intensity and broadens the linewidth of the InGaAs QW sample, while the 750 °C annealing shrinks the linewidth and enhances obviously the intensity of the InGaNAs sample. The PL peak shows up at 1.134 and 1.081 eV for the as-grown A-ag and B-ag, moves to 1.141 and 1.097 eV for the annealed A-600 and B-600, and 1.174 and 1.132 eV for the A-750 and B-750 samples. The 750 °C annealing induces an abrupt blueshift of the PL peak relative to that the 600 °C, and reduces the energy difference from 53 meV between the A-ag and B-ag to 42 meV between the A-750 and B-750 samples.

These phenomena reflect the N-induced effects in the InGaNAs and the influences of the RTA in the InGaAs and InGaNAs SQWs. To clarify the mechanisms behind, excitation-power, magnetic-field, and temperature dependent PL analyses are conducted.

A. Excitation-power dependent PL: Energy cross-over and linewidth broadening of two PL components

Excitation-power dependent PL measurements were carried out at 11 K. The representative PL spectra are depicted in Fig. 2 for the as-grown InGaAs (a) and InGaNAs (b)

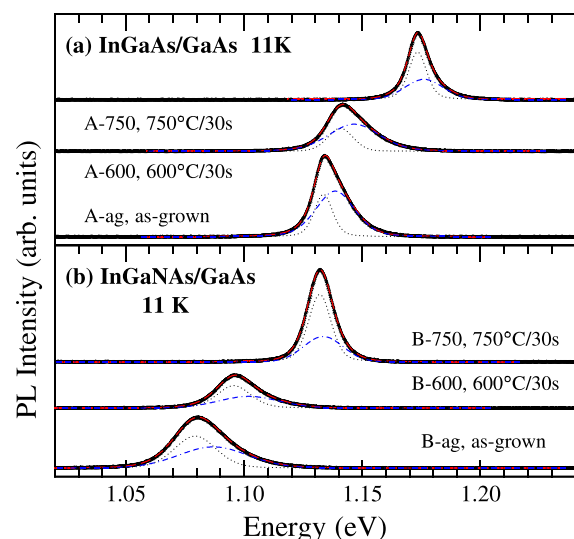


FIG. 1. PL spectra of (a) InGaAs/GaAs (A-ag, A-600, and A-750) and (b) InGaNAs/GaAs (B-ag, B-600, and B-750) SQWs at 11 K. Dots, dashed-dots, and dashes for curve fittings.

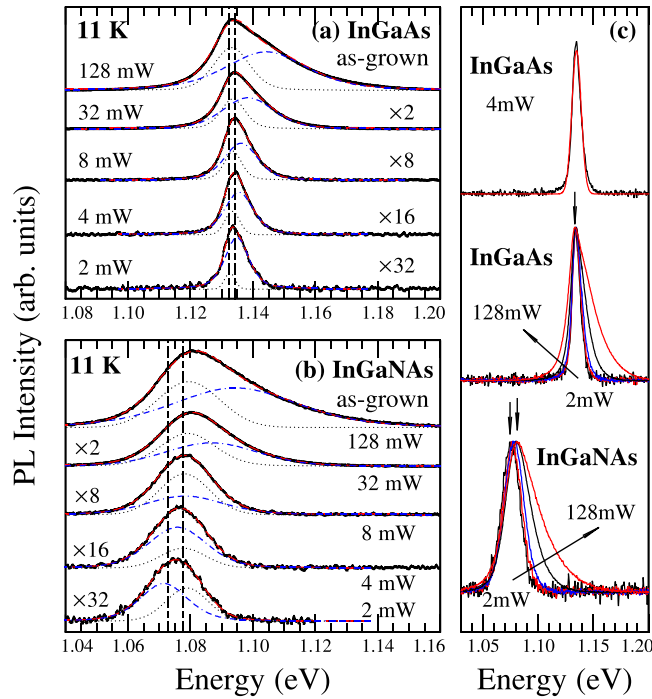


FIG. 2. Excitation power-dependent PL spectra of as-grown InGaAs/GaAs (a) and InGaNaS/GaAs (b) SQWs at 11 K, magnified to a similar peak height. Dots and dashed-dots for curve fittings, vertical dashes for PL-component peaks at 2 mW excitation. (c) The spectra are normalized and overlaid for the SQWs. Vertical arrows for main PL peak positions.

SQWs, respectively. The PL spectra are magnified for clear line shapes at lower excitation.

The linewidth of the InGaAs is significantly narrower than that of the InGaNaS, and both broaden as the excitation gets enhanced. The PL spectra are asymmetric, and can be fitted by two PL components with Gaussian profile as plotted in dots, dashed-dots, and dashes. The vertical dashes mark the energetic positions of the two PL components at an excitation of 2 mW. While one PL component keeps energetically unchanged (denoted with *standing-PL* component), the other moves to higher energies (denoted as *moving-PL* component) as the excitation power gets stronger. For the InGaAs SQW, the *moving-PL* component shows up on the high-energy side of the *standing-PL* component; for the InGaNaS SQW, however, the *moving-PL* component shows up on the low-energy side at low excitation, crosses over with the *standing-PL* component at about 8 mW, and moves up to the high-energy side as the excitation gets stronger further. To verify the rationality of the fittings, the PL spectra are normalized and overlaid in Fig. 2(c) for the as-grown InGaAs and InGaNaS samples, respectively. It is obvious that (i) even the rather symmetric PL spectrum of the InGaAs sample at 4 mW could not be fitted by single component satisfactorily; (ii) while the high-energy edge of the PL spectrum blueshifts significantly as the excitation power increases from 2 to 128 mW for the both samples, the low-energy edge of the PL spectrum redshifts slightly for the InGaAs sample but keeps nearly unchanged for the InGaNaS sample; and (iii) while the main PL peak position of the InGaAs sample does nearly not change with excitation power, that of the InGaNaS sample moves slightly and

gradually as the excitation rises up from 2 to 8 mW, but jumps to an obviously higher energy for the high excitation of 32 and 128 mW, as marked by the vertical arrows. This observation approves the two-component assumption, the different evolutions of the two components' positions for the two samples at relatively low excitation as well as a cross-over for the InGaNaS sample between 8 and 32 mW.

To reveal the evolution of the two PL components' energies with excitation power, a plot is drawn in Fig. 3 for the as-grown and annealed InGaAs (a) and InGaNaS (b) SQWs. The solid squares and open triangles represent the *standing-* and *moving-PL* components, while the dashes and solid lines serve as guides to the eyes. The data and the guide lines are shifted 10 meV downward for the as-grown samples for clarity.

The energy of the *standing-PL* component keeps nearly unchanged with the excitation power, while that of the *moving-PL* component shifts to higher energies monotonically and keeps at high-energy side in the whole excitation power range for the InGaAs SQWs. For the InGaNaS SQWs, however, there is a cross-over between the two PL components at about 8 mW. The blueshift of the *moving* component manifests nearly linear characteristic against the logarithm of the excitation power, $\ln P$. The energetic separation between the two PL components is about 11, 9, and 7 meV for the A-ag, A-600, and A-750 InGaAs, and 15, 16, and 7 meV for the B-ag, B-600, and B-750 InGaNaS SQWs at 128 mW, respectively.

The linewidth as a function of excitation power is depicted in Fig. 4 for the two PL components of the as-grown (a), 600 °C annealed (b), and 750 °C annealed (c) InGaAs (circles and open triangles) and InGaNaS (squares and filled triangles) SQWs. The dashes and solid lines serve as guides to the eyes. The scale of the vertical axis is set to an identical range of 0–70 meV. The values for the extremely low and

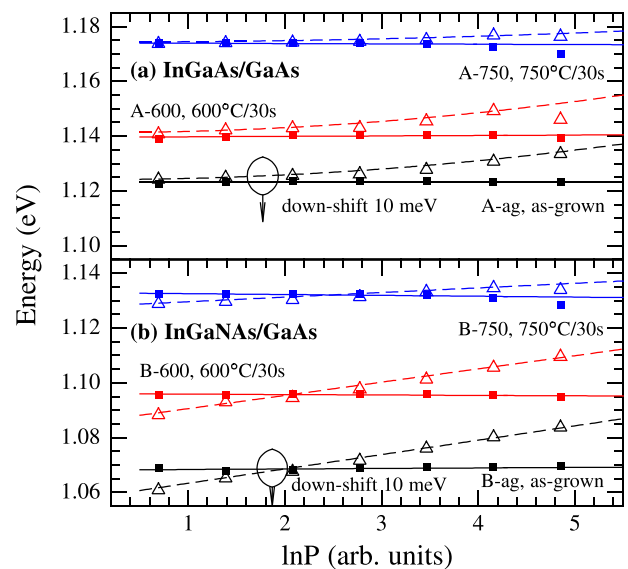


FIG. 3. Energy vs. excitation power for the PL components of as-grown and annealed InGaAs/GaAs (a) and InGaNaS/GaAs (b) SQWs at 11 K. Solid squares and open triangles for *standing-* and *moving-PL* components, 10-meV downshift for as-grown samples for clarity, dashes and solid lines for guiding the eyes.

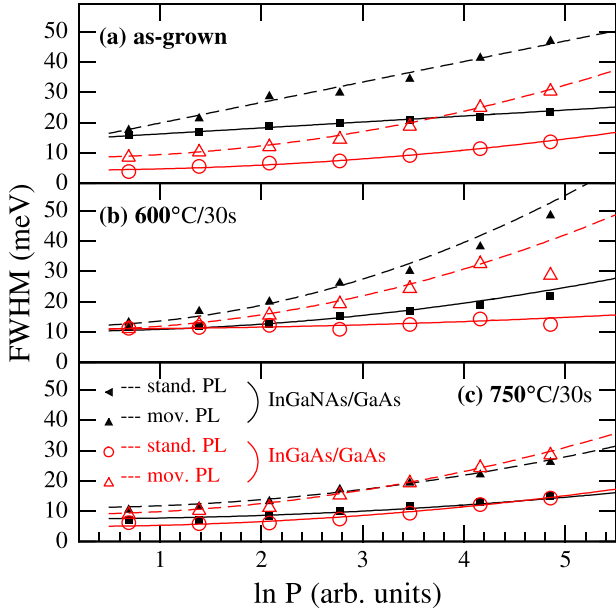


FIG. 4. Linewidth vs. excitation power for the two PL components of as-grown and annealed InGaAs/GaAs (circles and open triangles) and InGaNaNs/GaAs (squares and filled triangles) SQWs at 11 K. Dashes and solid lines guide the eyes.

high excitation (2 and 128 mW) are listed in Table I: at 2 mW, the linewidths of the *standing-* and *moving-PL* components are 4 and 9 meV, 11 and 12 meV, and 6 and 10 meV for the A-ag, A-600, and A-750 InGaAs; and 16 and 18 meV, 12 and 14 meV, and 7 and 11 meV for the B-ag, B-600, and B-750 InGaNaNs SQWs, respectively. At 128 mW, the corresponding values get to 14 and 31 meV, 13 and 30 meV, and 14 and 29 meV for the A-ag, A-600, and A-750 InGaAs; and 24 and 48 meV, 22 and 49 meV, and 15 and 27 meV for the B-ag, B-600, and B-750 InGaNaNs SQWs.

The phenomena indicate that (i) the PL lineshape is not dominated by below-gap bandtail states for the InGaAs SQW, as the *moving-PL* component shows up at high-energy side even at low excitation power; the annealing does not improve the PL intensity, and the annealing-induced blueshift is hence not the result of diminishing the bandtails as previously considered.¹⁷ (ii) The cross-over of the two PL components for the InGaNaNs SQW does not favor the bandtail assumption, and the annealing-induced narrowing and reduction of the two components' separation seem to be

TABLE I. FWHM of the *standing-* and *moving-PL* components for the InGaAs/GaAs (A-ag, A-600, and A-750) and InGaNaNs/GaAs (B-ag, B-600, and B-750) SQW samples at 11 K with excitation power of 2 and 128 mW, respectively.

Sample	FWHM (@2 mW)		FWHM (@128 mW)	
	standing-PL	moving-PL	standing-PL	moving-PL
A-ag	4	9	14	31
A-600	11	12	13	30
A-750	6	10	14	29
B-ag	16	18	24	48
B-600	12	14	22	49
B-750	7	11	15	27

inconsistent with the consideration of In-Ga interdiffusion and local nitrogen environment reorganization.³⁰ (iii) No Mott transition is seen even with the highest excitation power,²⁶ indicating the low-excitation characteristic of this measurement and the non-free-carrier transition of the *moving-PL* component.

For further insight in the *moving-* and *standing-PL* components, magneto-PL analysis is carried out.

B. Magneto-PL: Excitonic effect

Magneto-PL measurements were performed in a field range of 0–10 T at 4.5 K, with the magnetic field being perpendicular to the sample's surface. The excitation power was set at 80 mW to warrant the *moving-PL* component showing up on the high-energy side of the *standing-PL* component. The representative spectra are depicted in Fig. 5 for the 600 °C annealed InGaAs/GaAs (a) and InGaNaNs/GaAs (b) SQW samples, respectively. Vertical dashes indicate the main PL peak at $B = 0$ T, the main PL peak blueshifts obviously as the magnetic field rises, especially for the InGaAs SQW sample. The PL spectra show obvious asymmetric lineshape, and the two-component assumption applies for curve fittings. The results are plotted in dots and dashed-dots for the *standing-* and *moving-PL* components with Gaussian profile. The PL intensity is enhanced as the field gets higher especially for the InGaAs SQW and the *moving-PL* components, as depicted in Figs. 5(c) and 5(d) for the integral intensities of the *standing-PL* (sp), *moving-PL* (mp), and their summation (sp+mp) of the InGaAs and InGaNaNs SQW samples, respectively. Similar magnetic field-induced enhancement of oscillator strength (and hence integral intensity) was observed previously in InGaAs/InP quantum wells,

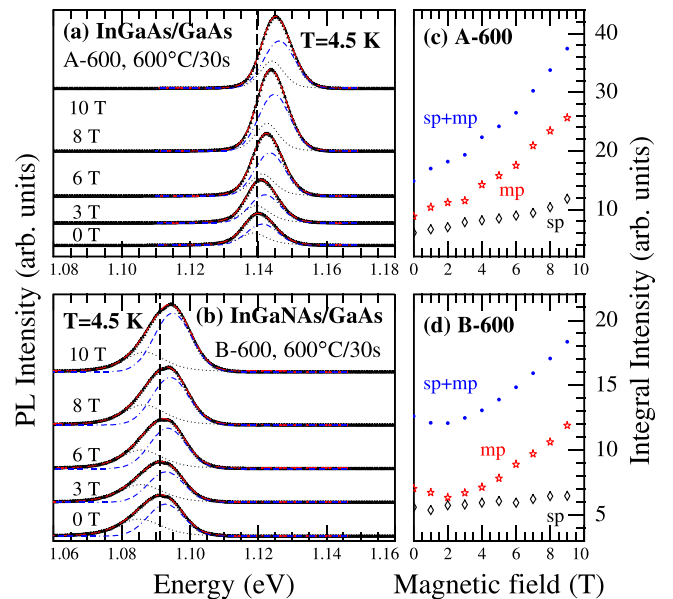


FIG. 5. Magneto-PL spectra of InGaAs/GaAs A-600 (a), InGaNaNs/GaAs B-600 (b), and corresponding integral intensities (c) and (d) at 4.5 K. Dots and dashed-dots in (a) and (b) for curve fittings, vertical dashes for peak position at 0 T. sp, mp, and sp + mp in (c) and (d) for *stand-*, *moving-PL*, and their summation.

and was shown to be due to the shrinkage of quasi-two-dimensional exciton wave functions.^{31,32}

Figure 6 plots the energies of the two PL components and the whole PL peak against magnetic field in squares, triangles, and open circles for the A-600 (a) and B-600 (b) SQWs. Similar to the PL peak, the two PL components manifest definitely blueshift with magnetic field, and the blueshift is relatively stronger for the A-600 SQW.

From theoretical viewpoint, the relative motion of the electron and hole constituting an exciton in QW is deformed by Lorentz forces when an external magnetic field B is applied to the exciton. For the exciton ground state with an S-like envelope wavefunction, the deformation leads to admixture with P-like envelope states. The resultant angular momentum is proportional to and antiparallel with B , the magnetic dipole's energy is also proportional to B .³³ The excitonic transition energy will therefore undergo a quadratic blueshift with B , which is known as *diamagnetic shift* and can be described quantitatively by a quasi-two-dimensional magneto-exciton model²⁹

$$\left\{ -\frac{\hbar^2}{2\mu} \left[\frac{1}{\rho} \frac{\partial}{\partial \rho} \left(\rho \frac{\partial}{\partial \rho} \right) \right] + \frac{e^2}{8\mu} B^2 \rho^2 + V(\rho) \right\} R(\rho) = ER(\rho),$$

$$V(\rho) = \frac{-e^2}{4\pi\epsilon_0} \int_{-\infty}^{+\infty} \int \frac{|Z_e(z_e)|^2 |Z_h(z_h)|^2}{\epsilon_r(z_e, z_h) \sqrt{\rho^2 + (z_e - z_h)^2}} dz_e dz_h, \quad (1)$$

where ρ is the in-well-plane separation between the electron and hole constituting an exciton. μ is the exciton reduced effective mass. $Z_e(z_e)$ and $Z_h(z_h)$ are the confined-state wavefunctions of electrons and holes, and are calculated by a model-solid method.³⁴⁻³⁶ $\epsilon_r \epsilon_0$ is the dielectric constant of the well or the barrier depending on z_e and z_h . $R(\rho)$ is excitonic envelope function. The theoretical excitonic energy shift is plotted in Fig. 6 as solid line and dashed-dots for the main

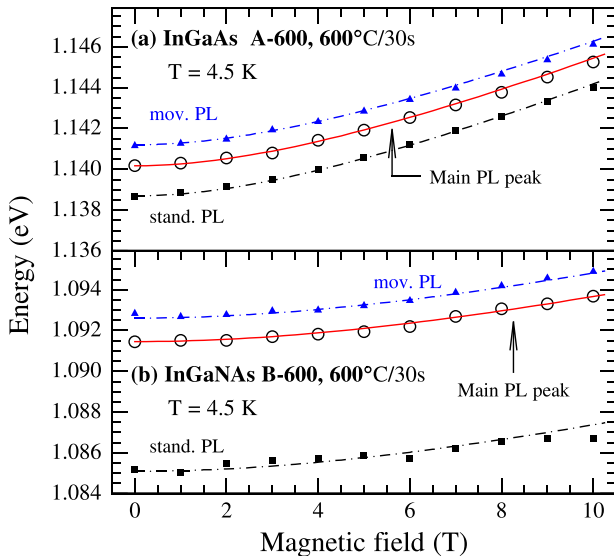


FIG. 6. Energy vs. magnetic field for (a) InGaAs/GaAs A-600 and (b) InGaAs/GaAs B-600 SQWs at 4.5 K. Lines and dashed-dots for theoretical excitonic diamagnetic shift.

PL peak and its two PL components, the good agreements with the experimental data indicate the excitonic nature of the two PL components. This is indeed consistent with the magnetic-field induced enhancement of the integral intensities as illustrated in Figs. 5(c) and 5(d). The exciton reduced effective mass and binding energy are derived as listed in Table II.

The InGaAs SQW samples have smaller E_b and μ than the corresponding InGaAs counterparts, the 600 °C annealing does not change the E_b and μ , while the 750 °C reduces the values significantly. For the InGaAs SQW, the 600 °C annealing drastically increases the E_b and μ , while the 750 °C reduces the values slightly relative to the as-grown sample. The as-grown and 600 °C annealed samples have slightly larger, while the 750 °C samples have smaller E_b and μ for the *moving-PL* components. These indicate that (i) the *standing-* and *moving-PL* components are not bandtail- and/or localization-related, but of similar interband exciton, due to the very similar excitonic parameters and the annealing-dependent energetic separation between the two components; (ii) annealing introduces different effects on the InGaAs and InGaAs SQWs; and (iii) the introduction of 1.2% nitrogen into InGaAs leads to an increased exciton binding energy by about 18%, 38%, and 15%, respectively, for the as-grown, 600 °C, and 750 °C annealed samples.

To trace out the real origin of the excitonic nature and the annealing effects, lineshape analysis of the PL spectra in a wide temperature range is conducted.

C. Temperature-dependent PL: Electron-phonon coupling

Temperature-dependent PL measurements were conducted with an excitation power of 32 mW to warrant the *moving-PL* component showing up on the high-energy side of the *standing-PL* component. The representative PL spectra are plotted in Fig. 7 for the as-grown InGaAs (a) and InGaAs (b) SQW samples in 11–290 K, respectively. The spectra of 150 K and above are magnified for tracing the PL peaks. The vertical dashed-dots mark the main PL peaks at 11 K, by which the redshift of PL peak is obvious for the temperatures above 40 K.

The PL spectra can be well fitted with the aforementioned two-component assumption as shown by dashes for the spectra taken at 11 K, by which the lineshape parameters of integral intensity, energy, and FWHM are obtained for

TABLE II. Exciton binding energy E_b in meV and reduced effective mass μ in m_e deduced from magneto-PL for InGaAs/GaAs (A-ag, A-600, and A-750) and InGaAs/GaAs (B-ag, B-600, and B-750) SQW samples.

Sample	Main E_b	Peak μ	<i>Standing</i> E_b^s	PL μ^s	<i>Moving</i> E_b^m	PL μ^m
A-ag	8.2	0.045	7.8	0.042	8.2	0.045
A-600	8.2	0.045	8.1	0.044	8.4	0.046
A-750	7.6	0.040	7.8	0.042	7.7	0.041
B-ag	9.7	0.056	9.6	0.055	9.8	0.057
B-600	11.3	0.071	11.2	0.070	11.3	0.07
B-750	8.7	0.048	9.3	0.053	8.4	0.046

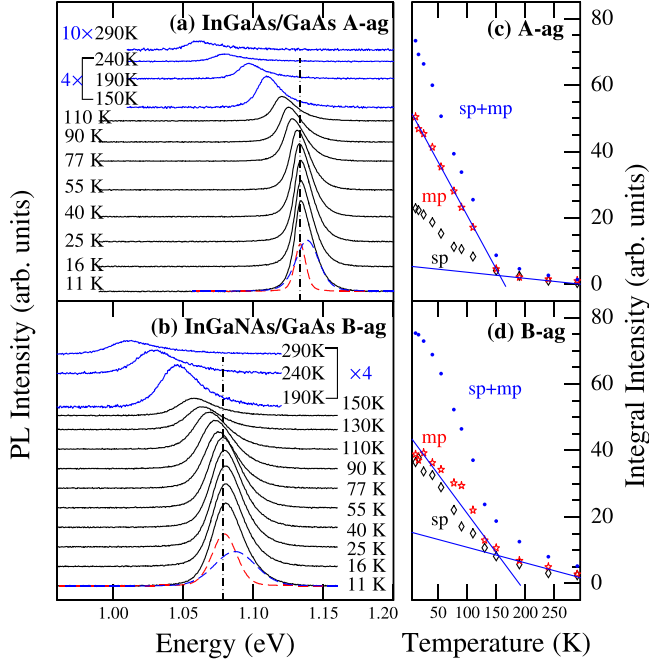


FIG. 7. PL spectra of as-grown InGaAs/GaAs (a), InGaNaS/GaAs (b), and corresponding integral intensities (c) and (d) in a temperature range of 11–290 K. Vertical dashed-dots in (a) and (b) mark peak position at 11 K, solid lines in (c) and (d) represent slopes of integral intensity vs. temperature.

each of the PL components, and the integral intensities of the *standing* (sp) and *moving* (mp) components as well as their summation (sp+mp) are plotted in Figs. 7(c) and 7(d) for the InGaAs and InGaNaS SQW samples, respectively. It is worthy to mention that though at low temperatures, the two components are both of the Gaussian profile, a mixture of Gaussian and Lorentzian is better for the *moving*-component in the temperature range above about 150 K, and finally a pure Lorentzian profile is necessary at 290 K. While inhomogeneous broadening has a Gaussian profile, homogeneous broadening has a Lorentzian profile, and LO-phonon scattering may dominate the broadening especially at higher temperatures.^{37,38} The temperature evolution of the integral intensity as shown in Figs. 7(c) and 7(d) is in fact consistent with the change of the lineshape that its quenching with temperature manifests a turning point at around 150 K as indicated by the slopes of the two parts of the integral intensity versus temperature.

Figure 8 depicts the energies of the main PL-peak, *standing*-, and *moving*-PL components as crosses, squares, and open triangles, respectively, for the InGaAs and InGaNaS SQWs. The data of the as-grown samples are shifted 20 meV downward for clarity.

The redshift with increasing temperature is the result of the band gap shrinkage, the latter is due primarily to the increase in the interatomic spacing and secondarily to the enhancement of carrier-phonon interaction as temperature increases. It can be quantitatively mimicked by an empirical formula as Varshni relation³

$$E_i(T) = E_i^0 - \frac{\alpha_i T^2}{T + \beta_i}, \quad (2)$$

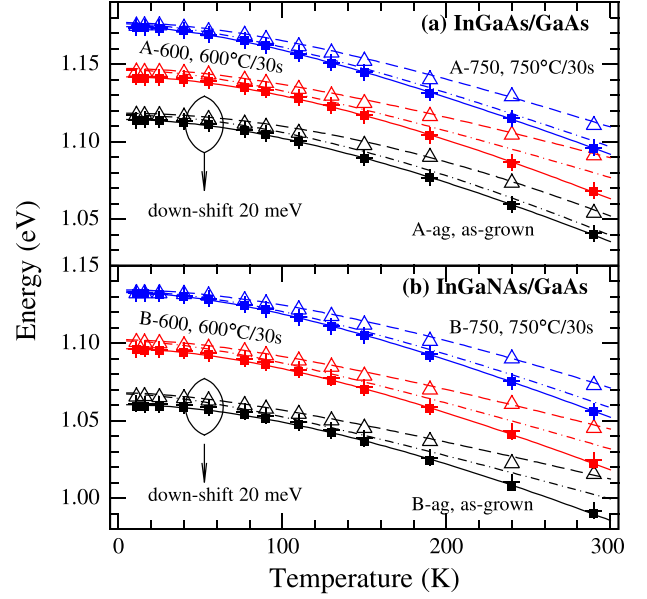


FIG. 8. Energy vs. temperature for the PL components of (a) InGaAs/GaAs and (b) InGaNaS/GaAs SQWs. Squares, open triangles, and crosses for *standing*-PL, *moving*-PL, and main PL peaks; dashes, solid lines, and dots for fittings by Varshni relation.

where i is for the main peak (p), *standing*- (s), and *moving*-PL (m), respectively. E_i^0 is the transition energy extrapolated to 0 K, α_i , and β_i are fitting parameters of a particular PL transition.³ The results are overlaid directly on the experimental data as dots, solid line (coincident with the dots), and dashes, respectively, for the main PL peak, *standing*-, and *moving*-PL components. The deduced parameters are listed in Table III for the *standing*-PL, *moving*-PL, and main PL peaks. To check if the evolution of the *moving*-PL component contains band/level thermal filling effects, additional fitting is made to the *moving*-PL component being subtracted by kT , and the result is depicted as dashed-dots in Fig. 8.

The main PL peak manifests similar characteristics of α_i and β_i as the corresponding *standing*-PL component for all the samples, the *moving*-PL, however, is rather different. The separation between the two PL components extrapolated to 0 K depends on annealing and has the smallest value of 2.6 and 1.7 meV for the 750 °C annealed InGaAs and InGaNaS SQW samples. The 750 °C annealed samples have also the smallest α_i and β_i for the main peak and *standing*-PL

TABLE III. Parameters of Varshni relation [Eq. (2)] for *standing*-PL (s), *moving*-PL (m), and main peak (p) energies of InGaAs/GaAs (A) and InGaNaS/GaAs (B) SQWs. E_p^0 and ΔE in meV for main peak energy and energy difference between the two PL components at 0 K. α in meV/K and β in K.

Sample	E_p^0	Main α_p	Peak β_p	<i>Standing</i> α_s	PL β_s	<i>Moving</i> α_m	PL β_m	ΔE
A-ag	1135.1	0.59	374	0.63	415	1.17	1277	4.1
A-600	1142.9	0.61	391	0.62	406	0.34	229	5.4
A-750	1174.4	0.46	205	0.46	201	0.42	254	2.6
B-ag	1081.6	0.66	498	0.62	448	0.28	147	7.6
B-600	1097.2	0.55	343	0.54	318	0.32	195	5.9
B-750	1133.0	0.52	281	0.50	260	0.49	391	1.7

component, and correspondingly, the largest main-peak redshifts of 78.2 and 76.4 meV for the InGaAs and InGaNaS SQWs, respectively, as the temperature changes from 11 to 290 K, relative to those of 74.1 and 72.5 meV for the 600 °C annealed and 74.1 and 69.5 meV for the as-grown samples. For the InGaAs SQW, the *moving-PL* manifests similar evolution of energy with temperature as the *standing-PL* for the as-grown and 750 °C annealed samples but weaker redshift than the *standing-PL* for the 600 °C annealed sample, if thermal filling effect is excluded from the *moving-PL* component; for the InGaNaS SQW, however, the *moving-PL* manifests weaker redshift than the *standing-PL* also for the as-grown sample.

Figure 9 illustrates the evolution of the FWHM with temperature. The open circles and triangles represent the *standing-* and *moving-PL* components of the InGaAs, while the solid squares and triangles for those of the InGaNaS SQWs. The *moving-PL* component shows broader FWHM than the corresponding *standing-PL*, and both broaden as temperature rises. The FWHMs of the as-grown InGaNaS are broader than the corresponding ones of the InGaAs SQW, the annealing reduces and that of 750 °C even eliminates the differences. For the InGaNaS SQW, annealing narrows the two PL components monotonically with raising the annealing temperature, while for the InGaAs SQW, 600 °C annealing even slightly broadens the PL components.

The broadening with temperature indicates phonon interaction and can be described by the phenomenological expression for electron-phonon interaction based on the Bose-Einstein statistical factor^{38–40}

$$\Gamma_i(T) = \Gamma_i^0 + \frac{\beta_i}{e^{(\hbar\omega_{LO})/kT} - 1}, \quad (3)$$

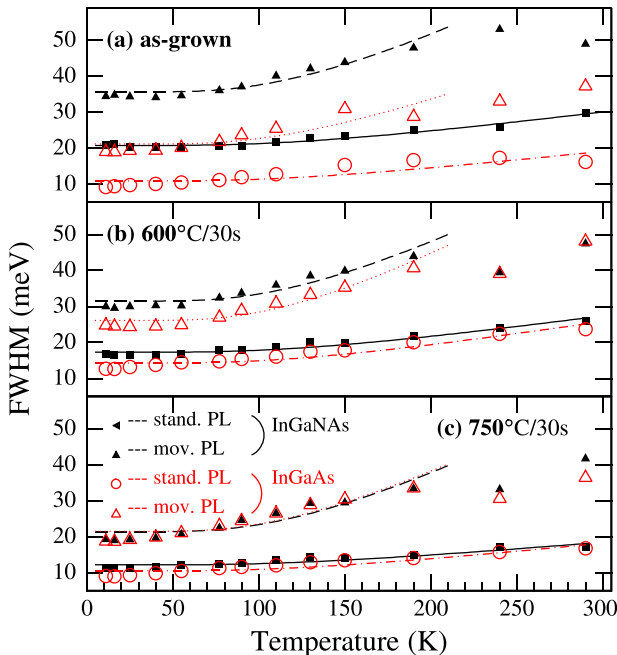


FIG. 9. FWHM vs. temperature for as-grown (a), 600 °C (b), and 750 °C (c) annealed SQWs. Open circles and triangles for *standing-* and *moving-PL* of InGaAs/GaAs; solid squares and triangles for those of InGaNaS/GaAs SQWs.

where i is for the *standing-* (s) or *moving-PL* (m) component, Γ_i^0 is the phonon independent part of Γ_i and related to the scattering with impurities and bound excitons. The second term arises from exciton scattering with optical phonons and β_i for the scattering strengths, $\hbar\omega_{LO}$ is the LO phonon energy of the QW layer and taken as a linear interpolation of the values 36.6, 29.6, 92.1, and 74.4 meV for GaAs, InAs, GaN, and InN.^{41,42}

The results for the *standing-* and *moving-PL* components are overlaid directly on the corresponding experimental data as solid lines and dashes for the InGaNaS, and dashed-dots and dots for the InGaAs SQWs, respectively. The fitting parameters are listed in Table IV. For the *standing-PL* component, the Γ_s^0 is 10.5–14.3 meV for the InGaAs, and 12.2–20.8 meV for the InGaNaS SQWs; annealing from 600 °C to 750 °C first slightly increases and then reduces the value for the InGaAs but reduces monotonically significantly for the InGaNaS SQWs. The β_s is in a similar range of around 20 meV, and shows similar annealing dependence of first increase and then decrease for the two SQWs. For the *moving-PL*, the Γ_m^0 is about double as the corresponding *standing-PL* component, and also first increases and then turns around as the annealing changes from 600 °C to 750 °C. The β_m is even about quadruple as that of the *standing-PL* component. While the *as-grown* InGaNaS SQW shows obviously larger Γ_i^0 and β_i values than the InGaAs SQW, the annealing of 750 °C significantly reduces and leads to similar values as the corresponding InGaAs SQW.

The evolution of energy and FWHM indicates that (i) both the *standing-* and *moving-PL* components originate in the inter-QW layer interband transition; the incorporation of N deteriorates the QW quality and broadens the FWHM, while the 750 °C annealing improves the quality and makes it comparable to the InGaAs SQW. (ii) The *standing-PL* component manifests similar redshift with temperature, while the *moving-PL* shows weaker redshift even when thermal filling effect is considered for the as-grown and 600 °C annealed, but similar redshift for the 750 °C annealed SQWs when the thermal filling effect is considered. This again disfavors the low-energy bandtail states, as otherwise the thermal filling should be more likely for the low-energy (here *standing-*) PL component. (iii) The *moving-PL* component corresponds to a stronger electron-phonon interaction than the corresponding *standing-PL*. The annealing slightly enhances the interaction for the InGaAs SQW but not for the InGaNaS SQW. For the both SQWs, the annealed samples show a similar strength of the interaction, hinting the

TABLE IV. Parameters of Eq. (3) for fitting the *standing-* and *moving-PL* line widths for as-grown and annealed InGaAs (A) and InGaNaS (B) SQWs. Γ_i^0 and β_i in unit of meV, and i for *standing* (s) and *moving* (m) components.

Sample	A-ag	A-600	A-750	B-ag	B-600	B-750
Γ_s^0	11.0	14.3	10.5	20.8	17.3	12.2
β_s	22.2	31.3	20.8	26.0	28.2	17.6
Γ_m^0	21.1	26.2	21.5	35.7	31.5	21.4
β_m	76.6	114.7	102.8	102.9	105.7	104.8

interaction to be in a different region of the QW layer for the *standing*- and *moving*-PL components, respectively.

D. Discussion

To well understand the experimental observations, neither the change of interlayer crystal quality nor the interdiffusion effects could be sufficient. Instead, a joint effect of intra-layer crystal quality, interfacial fluctuation of the quantum well layer, and interfacial diffusion has to be considered: (i) the InGaAs QW layer manifests fluctuation of In composition near the GaAs/InGaAs interface due to nonuniform In segregation,¹⁷ which can be described equivalently with a part of standard-thickness QW plus a part of slightly narrower QW, the latter leads to higher energy states for high temperature/excitation, and correspondingly the *moving*-PL component on the higher-energy side of the *standing*-PL component; (ii) incorporation of N in InGaAs degrades the intra-layer crystal quality and deteriorates the interfacial fluctuation,¹⁵ the former broadens the linewidth of each of the PL components, while the latter provides also lower energy states at low temperature/excitation and hence a cross-over of the *standing*- and *moving*-PL components at a medium excitation, and tends to enhance the separation of the two PL components at high excitation; and (iii) annealing at proper temperature improves the intra-layer crystal quality¹⁷ and drives interfacial In-Ga interdiffusion³⁰ along the vertical and horizontal directions, the former narrows the linewidth, while the latter weakens the In segregation, smooths the interfacial fluctuation, shrinks the effective QW-layer thickness, and hence leads to the blueshift and narrowing the separation of the two PL components.

To check if the interdiffusion-induced narrowing of the QW layer is qualified for the blueshift, the ground-state transition energy is calculated with a square-well assumption.⁴³ The band offset is determined by the model-solid method,^{34,35} and the dilute-N effect is estimated with the two-level repulsion model.^{44,45} Figure 10 depicts the transition energy of In_{0.375}Ga_{0.625}As/GaAs and In_{0.375}Ga_{0.625}N_{0.012}As_{0.988}/GaAs SQWs with the transition energy of 7-nm-thick In_{0.375}Ga_{0.625}As/GaAs SQW as reference.

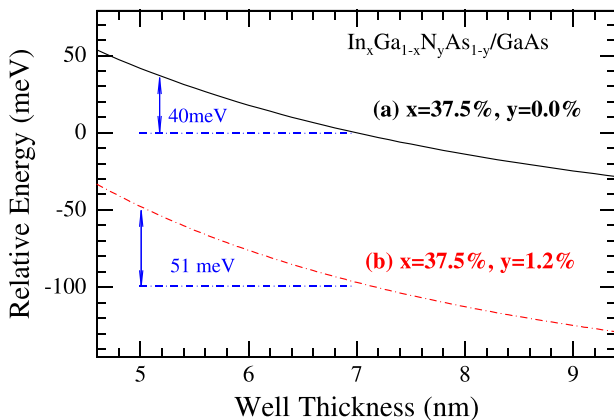


FIG. 10. Relative transition energy as a function of QW-layer thickness for In_xGa_{1-x}N_yAs_{1-y}/GaAs SQWs by model-solid method and two-level repulsion model, 7-nm-thick In_{0.375}Ga_{0.625}As/GaAs SQW as reference energy.

From the energy difference between the as-grown and annealed samples, the equivalent thickness of the InGaAs and InGaAs QW layers should shrink, respectively, to about 6.6 nm and 6.2 nm for the 600 °C, and 5.1 nm and 5.0 nm for the 750 °C annealed samples. Accordingly, the differences to the equivalent narrower QW parts of the InGaAs and InGaAs SQWs are, respectively, 0.5 and 0.7 nm for the as-grown, 0.4 and 0.8 nm for the 600 °C, and 0.3 nm for the 750 °C annealed samples.

Such amount of shrinkage is reasonable with respect to the previous studies. Liu *et al.* studied annealing effect on 8-nm-thick In_{0.372}Ga_{0.628}N_{0.015}As_{0.985}/GaAs SQW and concluded that annealing-induced interdiffusion length of ≤ 2 nm corresponds to PL peak blueshift of 18–28 meV.²⁵ Bouragba *et al.* indicated that while a nitrogen free InGaAs/GaAs SQW sample shows the In-Ga interdiffusion, the introduction of nitrogen moderately enhances the phenomenon.³⁰ Shirakata *et al.* indicated that for 10-nm-thick In_{0.32}Ga_{0.68}N_{0.01}As_{0.99}/GaAs SQW, annealing improves the crystal quality to be comparable with that of corresponding N-free sample.²⁴ Lai *et al.* showed for 6-nm-thick In_{0.34}Ga_{0.66}N_xAs_{1-x}/GaAs SQWs, the PL peak energy manifests a pronounced temperature-dependent S-shaped for the dilute-N samples at low temperatures,²² while it follows the empirical Varshni model in the high-temperature region with significant reduction in the temperature dependence as compared to the N-free sample, the latter manifests similar α and β values as those of the main PL peaks for the A-ag and B-600/B-750 as listed in Table III.

It is noteworthy that (i) a study of RTA effects on InGaAs/GaAs SQWs correlated the annealing-induced blueshift to the N content in the QW layer but not the In interdiffusion,²³ which seems to be contrary to the above discussion. Note, however, that the reference N-free sample manifested significantly smaller blueshift, which is not the case in the present study. (ii) For a similar narrowing of the QW layer, while 40 and 51 meV blueshift is predicted for 7-nm-thick InGaAs and InGaAs SQWs, respectively, much reduced values of 24 and 27 meV are expected if the QW layer is 9 nm, which are very closed to the previous reports.^{23–25} (iii) A density-dependent time-resolved PL study of a 8 nm InGaAs/GaAs SQW derived an exciton binding energy of about 6.5 meV,²⁶ and a lineshape analysis-assisted temperature-dependent PL study of 6 nm In_{0.4}Ga_{0.6}As/GaAs deduced an exciton binding energy of about 9.7 meV,²⁷ both are very similar to those as listed in Table II. Nevertheless, a drastic enhancement of excitonic effect by dilute nitrogen was suggested and a very low N content of about 0.5% was considered to increase surprisingly the exciton binding energy in the 6 nm In_{0.4}Ga_{0.6}N_{0.005}As_{0.995}/GaAs by 80% relative to the referential InGaAs/GaAs SQW to 17.5 meV,²⁷ which is obviously inconsistent with those as listed in Table II. Note, however, that the lineshape analysis was based on a two-component assumption of additive of excitonic and free-carrier transitions and the exciton binding energy was derived indirectly with a plot of the ratio of free carriers to exciton populations against $1/k_B T$,²⁷ this is, however, in clear contrast to the nature of two excitonic components and the direct derivation of the exciton binding energy by diamagnetic shift in this study. (iv) As the QW interdiffusion has been applied as a post-growth

approach for engineering the bandgap on selected areas to achieve monolithic integration of different optoelectronic functions,^{46,47} the effect of the interfacial fluctuation of either thickness or composition deserves special attention in the annealing-induced bandshift engineering.

IV. CONCLUSION

To conclude, for the InGa(N)As/GaAs SQWs not showing *S-shape* evolution of PL-peak energy with temperature, the PL spectra at different excitation powers, temperatures and magnetic fields can be well fitted by a two-PL-component assumption, and the PL components are both excitonic and of interband ground-state related transition in the QW portions with slightly different well thicknesses. The RTA introduces similar levels of blueshift and narrowing to the PL components of the both InGa(N)As SQWs with and without N content, and the mechanisms behind the annealing effects are inferred that (i) the In segregation near the interface causes less-In QW region, which corresponds equivalently to higher-energy states and hence the high-energy *moving-PL* component, N introduces additional fluctuation to the interface and provides also lower-energy states, as shown by the excitation power-dependent PL analysis in Sec. III A; (ii) the annealing improves the intra-layer crystal quality and hence narrows the PL components, as indicated by the excitation power-dependent PL analysis in Sec. III A and the temperature-dependent PL analysis in Sec. III C. It also enhances the interfacial In-Ga interdiffusion and leads to an equivalent reduction of the QW thickness and interface fluctuation, and hence the blueshift of the PL components and reduction of the PL-components' separation as revealed by the temperature-dependent PL analysis in Sec. III C; and (iii) the interfacial In-Ga interdiffusion does not change obviously by the small amount N content (here is about 1.2%) and hence similar levels of PL-component narrowing and blueshift are observed after a nominally identical RTA treatment. The introduction of 1.2% nitrogen into InGaAs increases the exciton binding energy by a moderate level of about 15% for the 750 °C annealing as derived by the magneto-PL analysis in Sec. III B.

As for neither of the InGa(N)As SQWs does the bandtail explicitly show up even at rather low excitation power/temperature, the as-grown SQWs do already possess very good optical quality and hence the interfacial effects play an important role in the evolution of the PL lineshape with excitation, temperature, and magnetic field. From this viewpoint, PL measurements with sufficient spectral resolution and SNR together with lineshape analysis will be desirable and informative for probing the interfacial modification by annealing.

ACKNOWLEDGMENTS

The work was supported by the MOST 973 Program (2014CB643901 and 2013CB632805), the STCSM (11JC1413800), and the NSFC (61176075, 11274329, and 61290302) of China.

- ¹J. Shao, R. Winterhoff, A. Dömen, E. Baars, and J. Chu, *Phys. Rev. B* **68**, 165327 (2003).
- ²J. Shao, W. Lu, X. Lü, F. Yue, Z. Li, S. Guo, and J. Chu, *Rev. Sci. Instrum.* **77**, 063104 (2006).
- ³Y. P. Varshni, *Physica* **34**, 149 (1967).
- ⁴K. P. O'Donnell and X. Chen, *Appl. Phys. Lett.* **58**, 2924 (1991).
- ⁵G. Ortner, M. Schwab, M. Bayer, R. Pässler, S. Fafard, Z. Wasilewski, P. Hawrylak, and A. Forchel, *Phys. Rev. B* **72**, 085328 (2005).
- ⁶M. Hugues, B. Damilano, J.-Y. Duboz, and J. Massies, *Phys. Rev. B* **75**, 115337 (2007).
- ⁷J. Shao, X. Lü, F. Yue, W. Huang, S. Guo, and J. Chu, *J. Appl. Phys.* **100**, 053522 (2006).
- ⁸J. Shao, L. Chen, W. Lu, X. Lu, L. Zhu, S. Guo, L. He, and J. Chu, *Appl. Phys. Lett.* **96**, 121915 (2010).
- ⁹X. Zhang, J. Shao, L. Chen, X. Lü, S. Guo, L. He, and J. Chu, *J. Appl. Phys.* **110**, 043503 (2011).
- ¹⁰X. Chen, Y. Song, L. Zhu, S. M. Wang, W. Lu, S. Guo, and J. Shao, *J. Appl. Phys.* **113**, 153505 (2013).
- ¹¹J. N. Baillargeon, K. Y. Cheng, G. E. Hofler, P. J. Pearah, and K. C. Hsieh, *Appl. Phys. Lett.* **60**, 2540 (1992).
- ¹²M. Kondow, K. Uomi, A. Niwa, T. Kitatani, S. Watahiki, and Y. Yazawa, *Jpn. J. Appl. Phys. Part 1* **35**, 1273 (1996).
- ¹³N. Tansu, J.-Y. Yeh, and L. J. Mawst, *Appl. Phys. Lett.* **83**, 2512 (2003).
- ¹⁴X. Wang, S. M. Wang, Y. Q. Wei, M. Sadeghi, and A. Larsson, *Electron. Lett.* **40**, 1338 (2004).
- ¹⁵M. M. Oye, T. J. Mattord, G. A. Hallock, S. R. Bank, M. A. Wistey, J. M. Reifsnider, A. J. Ptak, H. B. Yuen, J. S. Harris, and A. L. Holmes, *Appl. Phys. Lett.* **91**, 191903 (2007).
- ¹⁶I. A. Buyanova, W. M. Chen, G. Pozina, J. P. Bergman, B. Monemar, H. P. Xin, and C. W. Tu, *Appl. Phys. Lett.* **75**, 501 (1999).
- ¹⁷H. Zhao, S. M. Wang, Q. X. Zhao, Z. H. Lai, M. Sadeghi, and A. Larsson, *Semicond. Sci. Technol.* **23**, 125002 (2008).
- ¹⁸J. C. P. Chang, J. M. Woodall, M. R. Melloch, I. Lahiri, D. D. Nolte, N. Y. Li, and C. W. Tu, *Appl. Phys. Lett.* **67**, 3491 (1995).
- ¹⁹Y. Kajikawa, N. Nishimoto, D. Fujioka, and K. Ichida, *Jpn. J. Appl. Phys. Part 1* **45**, 2412 (2006).
- ²⁰H. Zhao, Y. Q. Xu, H. Q. Ni, S. Y. Zhang, D. H. Wu, Q. Han, R. H. Wu, and Z. C. Niu, *J. Appl. Phys.* **99**, 034903 (2006).
- ²¹A. Matsumoto, A. Matsushita, Y. Takei, K. Akahane, Y. Matsushima, H. Ishikawa, and K. Utaka, *Appl. Phys. Express* **7**, 092801 (2014).
- ²²F.-I. Lai, S. Y. Kuo, J. S. Wang, H. C. Kuo, S. C. Wang, H. S. Wang, C. T. Liang, and Y. F. Chen, *J. Vac. Sci. Technol. A* **24**, 1223 (2006).
- ²³V. Liverini, A. Rutz, U. Keller, and S. Schön, *J. Appl. Phys.* **99**, 113103 (2006).
- ²⁴S. Shirakata, M. Kondow, and T. Kitatani, *Appl. Phys. Lett.* **80**, 2087 (2002).
- ²⁵H. F. Liu, V. Dixit, and N. Xiang, *J. Appl. Phys.* **99**, 013503 (2006).
- ²⁶L. Kappei, J. Szczytko, F. Morier-Genoud, and B. Deveaud, *Phys. Rev. Lett.* **94**, 147403 (2005).
- ²⁷L. Xu, D. Patel, C. S. Menoni, J. Y. Yeh, L. J. Mawst, and N. Tansu, *Appl. Phys. Lett.* **89**, 171112 (2006).
- ²⁸L. Zhu, J. Shao, X. Lü, S. Guo, and J. Chu, *J. Appl. Phys.* **109**, 013509 (2011).
- ²⁹J. Shao, D. Haase, A. Dörnen, V. Härle, and F. Scholz, *J. Appl. Phys.* **87**, 4303 (2000).
- ³⁰T. Bouragba, M. Mihailovic, F. Reveret, P. Disseix, J. Leymarie, A. Vasson, B. Damilano, M. Hugues, J. Massies, and J. Y. Duboz, *J. Appl. Phys.* **101**, 073510 (2007).
- ³¹M. Sugawara, *Phys. Rev. B* **45**, 11423 (1992).
- ³²I. Aksenov, J. Kusano, Y. Aoyagi, T. Sugano, T. Yasuda, and Y. Segawa, *Phys. Rev. B* **51**, 4278 (1995).
- ³³C. Klingshirn, *Semiconductor Optics*, 2nd ed. (Springer-Verlag, Berlin Heidelberg, 2005).
- ³⁴C. G. V. de Walle, *Phys. Rev. B* **39**, 1871 (1989).
- ³⁵J. Shao, A. Dörnen, R. Winterhoff, and F. Scholz, *Phys. Rev. B* **66**, 035109 (2002).
- ³⁶I. Vurgaftman and J. R. Meyer, *J. Appl. Phys.* **94**, 3675 (2003).
- ³⁷J. Humlíček, E. Schmidt, L. Bočánek, R. Švehla, and K. Ploog, *Phys. Rev. B* **48**, 5241 (1993).
- ³⁸J. Shao, W. Lu, G. K. O. Tsen, S. Guo, and J. M. Dell, *J. Appl. Phys.* **112**, 063512 (2012).
- ³⁹P. Lautenschlager, M. Garriga, L. Vina, and M. Cardona, *Phys. Rev. B* **36**, 4821 (1987).
- ⁴⁰H. Qiao, K. A. Abel, F. C. J. M. van Veggel, and J. F. Young, *Phys. Rev. B* **82**, 165435 (2010).

- ⁴¹R. Heitz, M. Grundmann, N. N. Ledentsov, L. Eeckey, M. Veit, D. Bimberg, V. M. Ustinov, A. Y. Egorov, A. E. Zhukov, P. S. Kopçev, and Z. I. Alferov, *Appl. Phys. Lett.* **68**, 361 (1996).
- ⁴²C. Bungaro, K. Rapcewicz, and J. Bernholc, *Phys. Rev. B* **61**, 6720 (2000).
- ⁴³J. Shao, A. Dörnen, E. Baars, V. Härle, F. Scholz, S. Guo, and J. Chu, *J. Appl. Phys.* **93**, 951 (2003).
- ⁴⁴W. Shan, W. Walukiewicz, J. W. Ager III, E. E. Haller, J. F. Geisz, D. J. Friedman, J. M. Olson, and S. R. Kurtz, *Phys. Rev. Lett.* **82**, 1221 (1999).
- ⁴⁵J. Shao, W. Lu, M. Sadeghi, X. Lü, S. M. Wang, L. Ma, and A. Larsson, *Appl. Phys. Lett.* **93**, 031904 (2008).
- ⁴⁶K.-H. Lee, K. Thomas, A. Gocalinska, M. Manganaro, E. Pelucchi, F. H. Peters, and B. Corbett, *J. Appl. Phys.* **112**, 093109 (2012).
- ⁴⁷R. Beal, V. Aimez, and J. J. Dubowski, *Opt. Express* **23**, 1073 (2015).